Correlation Between Tensile Strength & Modulus of Rupture for Ultra High-Performance Concrete (UHPFRC)

Zoi Ralli Ph.D. Candidate, York University. (416-848-9099), zoiralli@yorku.ca
Stavroula J. Pantazopoulou, Ph.D., Professor, York University. pantazo@yorku.ca

ABSTRACT

The increased use of ultra-high-performance concrete as an alternative to conventional concrete in bridge construction and infrastructure has brought forth the need for reliable assessment of the actual mechanical properties from samples taken during preparation of the mix and in the field during placement of the material. Particular interest is in the tensile strength and tensile strain ductility of UHPFRC that effectively limits crack propagation and minimizes the width of cracks, which in turn greatly improves the durability of the structure. However, design standards face the conundrum that whereas direct tensile tests would be ideal for characterization of tensile strength and resilience, yet these tests are very difficult to conduct. Instead, what has prevailed is the flexural prismatic beam test, where the tensile strength and tensile stress-strain properties of the material are derived through inverse analysis. An important concern arises from this state of practice: material strengths calculated from flexural tests are routinely several fold the values obtained from direct tension tests. Objective of the paper is to correlate through detailed finite element analysis the mechanics and state of stress of the different test setups so as to establish the relevance of the experimental results with the intrinsic tensile strength of the material. Particular emphasis is placed on the influence of experimental configuration on the response of specimens subjected to four-point bending.

INTRODUCTION

The experimental characterization of the tensile strength of UHPFRC is mainly based on procedures in codes and standards used for fiber reinforced concrete (FRC). The most reliable, and yet most difficult to conduct test for determining the tensile behaviour is the direct tension test. The specimen is usually a prism subjected to uniaxial tension and characteristics such as distribution, spacing and width of cracks should be recorded at ultimate stress. The variation in geometry, boundary conditions and size of the specimens complicates the development of a standard test and prevent correlation between different studies.

A common practice is to evaluate the tensile behaviour indirectly, through tests that are controlled by some form of tensile failure. For example, tensile strength of FRC's is often obtained through variations of the well-known Brazilian splitting test, where a cylindrical specimen is subjected to compressive load, along two diametrically opposed generating lines of the cylinder. Uniform transverse tensile stress state is generated almost lengthwise the diameter plane that is parallel to the applied loads. Failure occurs once the tensile strength of the material is reached. Despite the simplicity of the experimental setup and procedure, uncertainty arises regarding the actual stress distribution.

Led by the necessity to overcome the intrinsic difficulties of conducting direct tension tests, several codes and standards adopted flexural tests (i.e. modulus of rupture tests), either in three-point or four-point bending as an alternative way to evaluate the tensile behaviour of the material. They are used to determine toughness parameters and thus establishing the post tensile and strain hardening behaviour. Through an inverse analysis, the constitutive relationship of uniaxial tensile stress versus crack opening is calculated from the flexural test results. Several back-calculation approaches are available in the literature from various standards and researchers. However, the majority of them leads to overestimation of the true tensile strength, due to simplifying assumptions regarding the kinematics of the bending problem and the material behavior.

Three-point bending tests in several standards are usually performed on notched specimens with the exception of ASTM C293/293M[1] which is an unnotched three-point bending test. The specimen with specified dimensions and a deep notch at midspan is placed in a center-point loading configuration. When the flexural strength is reached at the tip of the crack, one single crack initiated by the notch propagates and the absorbed energy is assumed to be entirely due to the fracture along the notch. Therefore, for the characterization of the behaviour, flexural toughness or load versus crack mouth opening displacement

(CMOD) could be used. Although notched three-point bending test is suitable for material characterization of FRCs, it is not recommended to assess reliably the strain-hardening behaviour of UHPFRC. Multi-microcracking that may appear around the notch hinders conventional inverse analyses proposed by RILEM and MC2010 as they assume that CMOD is due to the opening of a single crack. This leads to overestimation of tensile properties of strain hardening UHPRFC, and thus notched three-point bending tests should be generally avoided.

Unnotched four-point bending test have prevailed in codes and standards. The main advantage of the test configuration is the constant bending moment in the central part of the span, between the point loads. However, the length to height ratio of the specimen affects the stress field as the lower it goes the stronger is the influence of the stress disruption under the point loads. For simplicity, the latter effect is neglected and the strain-hardening behaviour is determined through the load vs midspan displacement curve according to a smeared crack approach. The most common version of four-point bending test is the third point bending test, where the distance between the point loads is equal to one third of the beam span. Unnotched four-point bending test is considered less biased than the three-point option, and therefore more appropriate for UHPFRC as the failure will take place in the weakest section and not under the point load.

So far, French (AFNOR) and Swiss standards are the only standards that include tensile properties tests especially for UHPFRC. A direct tension test is proposed in Swiss standard, whereas French Standards recommend a notched three-point bending test. However, both standards have also an unnotched four-point bending test for UHPFRC. According to AFNOR[2], there are three types of UHPFRC: (i) strain-softening, (ii) low strain-hardening and (iii) high strain-hardening. For the first two categories, two different tests should be conducted. Firstly, a third point bending test is required for the establishment of cracking strength. Following the assumption that the first crack can be visually distinguished at the point where significant loss of linearity takes place, the cracking strength is determined. The second test to be performed is a notched three-point bending test with recording of the CMOD at crack strength. The next step is a point-by-point inverse analysis used to derive the post-cracking behaviour. Although the process described above seems to be easy, the subjective nature of the first cracking strength determination and the untrue - for strain hardening materials - kinematic assumption of linear curvature distribution during loading and unloading may lead to inaccurate results. The last class refers to the strain-hardening response of UHPFRC, which is investigated through an unnotched third point bending test on a thin specimen. The bilinear stress-strain behaviour is determined through a point-by-point simplified inverse analysis method.

The Swiss standard, on the other hand, does not suggest different tests for the different UHPFRC types. Direct tension test and third point bending test are proposed, and it is required that both be performed. The direct tension test involves a dog-bone shaped specimen with specific geometry and a fixed end boundary condition. The flexural test specimen should have also specified dimensions and during the test, load-displacement at midspan should be recorded, in order to obtain a bilinear tensile stress-strain hardening response through a simplified inverse analysis procedure.

In order to determine the tensile properties of UHPFRC, the results obtained from the indirect tests proposed above have to be used in inverse analysis. The available approaches aim to reproduce the experimental results by implementing numerical models based on predetermined model forms of the uniaxial tensile and compressive stress-strain relationships. Thus, inverse analysis enables determination of the model parameters, rather than revealing the intrinsic tensile properties. This is particularly true for methods that are based on experimental points from tests; these are known as simplified methods.

Inverse analysis is fraught with the uncertainties necessarily introduced in the analysis of a model with the intent to match the experimental evidence; these include kinematic assumptions implicitly made when defining strain-displacement relationships, stress-strain models for the response of the specimen in the compression zone but also the assumed form of the tensile stress-strain envelope. A very important aspect is the actual degree of restraint provided at the supports and at the load points. To understand the significance of these variables on the expected results, this paper uses detailed finite element analysis to correlate the mechanics and state of stress of the different test setups that are routinely used in the literature so as to establish the sensitivity of the responses obtained to the intrinsic tensile behavior of the material.

A BRIEF REVIEW OF THE STATE OF THE ART

The degree of uncertainty in estimating the tensile strength of UHPFRC materials is depicted in Figure 1 which plots experimentally obtained tensile strength values for three different UHPCFRC materials using

direct tension tests and inverse analyses[3] (Yang, 2019); the latter was conducted using the method of Lopez[4], (Lopez, 2017) which was adopted in the CSA A23.1 Code[5] (CSA, 2019). The scatter of the results below the equal value line is points to a systematic overestimation of tensile strength obtained from inverse analysis as compared to the direct tension testing. Apart from the evident need of introducing pertinent safety factors when flexural tests are used to define the tensile strength property, the figure underscores the limited understanding currently available regarding the true tensile strength of UHPFRC. Note that the source of the discrepancy is not necessarily owing to the misleading attributes of the flexural test: direct tension tests are also criticized for their lack of the ability to recover a near uniform stress distribution after initiation of cracking from either edge on account of the acute eccentricity which is thus generated (Fig. 2a). In addition, owing to the thin spacing in the grips that are usually available in Universal Testing Frames, direct tension tests are likely to have a fiber distribution that is intensely two-dimensional as compared to the three-dimensional fiber distribution that may be attained in flexural prisms.
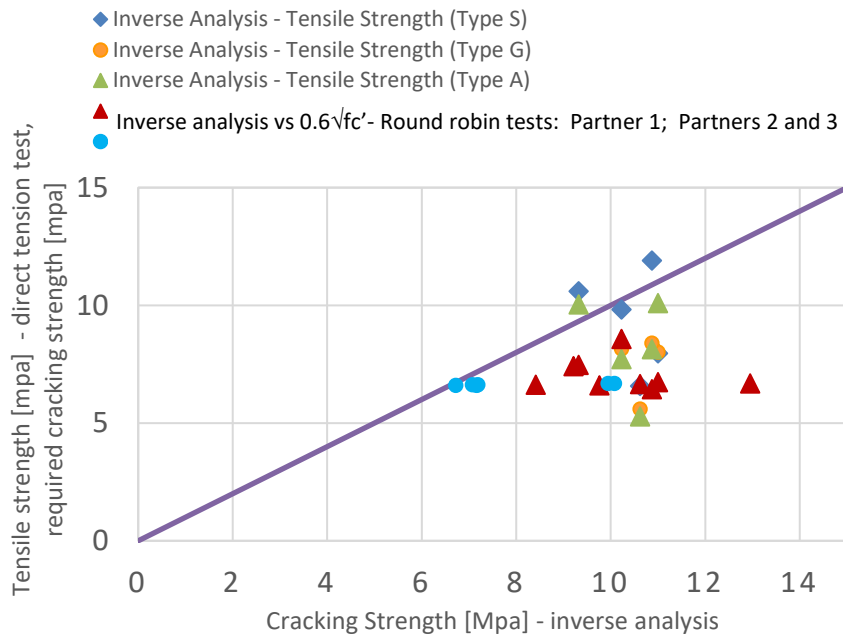

Figure 1: Comparison of results of direct tension tests and tensile strength values obtained from inverse analysis on tests conducted by three different test labs on the same UHPRFC materials (casting of specimens from a single mix by Partner 1). (Each point averages three identical specimens). Red and light blue circles compare results of inverse analysis with the estimate for cracking strength = $0.6\sqrt{f_c'}$.
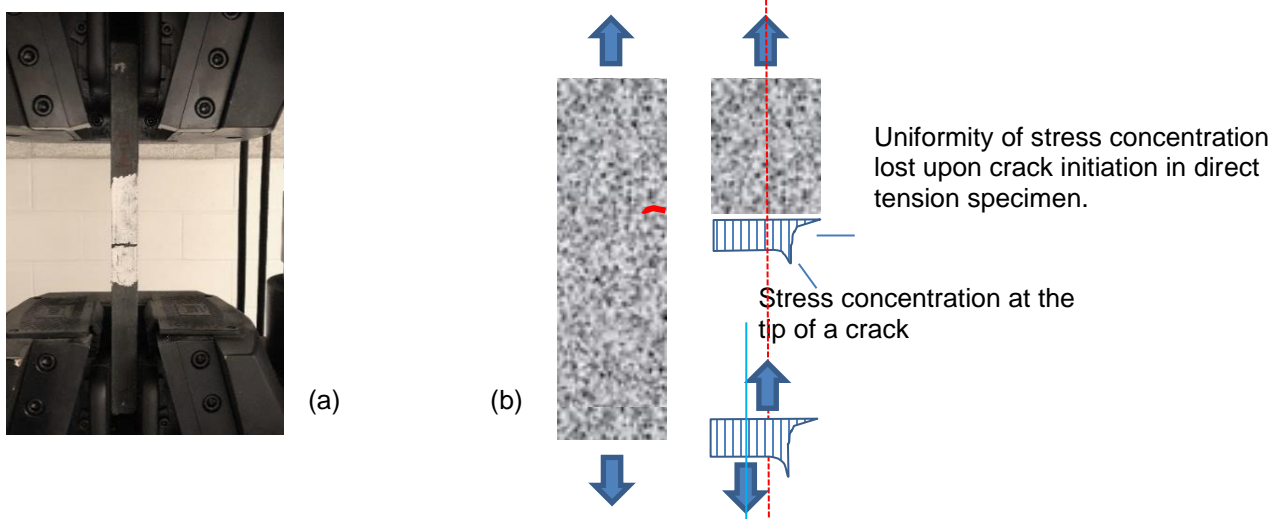

Figure 2: (a) Typical Direct Tension Arrangement – Side View: The specimen thickness is dictated by the available spacing of the grip (b) Eccentricity in direct tension specimen owing to the crack initiation leads to precipitous failure.

Inverse analysis conducted according to the simplified methods included in the codes (e.g. RILEM TC 162-TDF and MC2010) are straightforward but may lack accuracy. Both depend on the use of notched three-point bending test results according to EN-14651. Alternatives to these are approaches that rely on detailed finite element analysis to obtain the complete stress strain response – either iteratively, or through a point-by-point process have also been tried: in the former, the form of a constitutive model is assumed, while its parameters are determined through matching of experimental and analytical results; the latter approaches build progressively in each step the constitutive law.

In the simplified approach, the load-midspan deflection curve is obtained from flexural tests under monotonically increasing load. In strain hardening materials there is a range that is mildly ascending past the end of the linear range, identified by points P_y and Δ_y. This strain hardening range increases up to a peak load value P_{max} and a corresponding displacement Δ_{max}. Past the peak point initially there is a mild descend, at point P_u, Δ_u, which is associated with the onset of cracking localization and subsequent post peak descend in the response curve as the governing crack width grows. Load is converted into moment in the critical region (maximum moment in the beam between the point loads) through statics for known shear span length a (distance between support and impactor shafts); so $M_y=0.5{\cdot}a{\cdot}P_y$; $M_{max}=0.5{\cdot}a{\cdot}P_{max}$; and $M_u=0.5{\cdot}a{\cdot}P_u$. However, conversion of displacement to average curvature is less obvious unless both displacements at midspan and at both loading points are available through direct LVDT measurements. Here therefore is a primary source of uncertainty in simplified inverse analysis, since it is necessary to make an underlying assumption regarding the form of the strain-displacement relationship in the midspan, in order to reduce the displacement values into curvature at the critical section. Few researchers have reported results of this type obtained by a series of LVDTs [6](Baby et al, 2012). With the average strain is recorded with two LVDTs on the tension face in the segment between the point loads, then by assuming linear elastic behaviour in compression, stress equilibrium was established at midspan for each experimental pair of load-strain values, thereby building the tensile stress-strain law point-by-point. However, the prevalent assumption is to linearize the curvature distribution as depicted in Fig. 3(a) for stages that correspond to milestone events in the resistance curve either prior to, or after cracking[7,8] (Qian et al, 2007, Riguad et al, 2011). According to Georgiou and Pantazopoulou[9] (Georgiou and Pantazopoulou, 2017) the last of the points, should be taken to be very close to the maximum value in the post-peak: this point corresponds to tension crack penetration from the tension face by such an amount that it is the resultant moment M_u can no longer be supported (Fig. 3(c)).
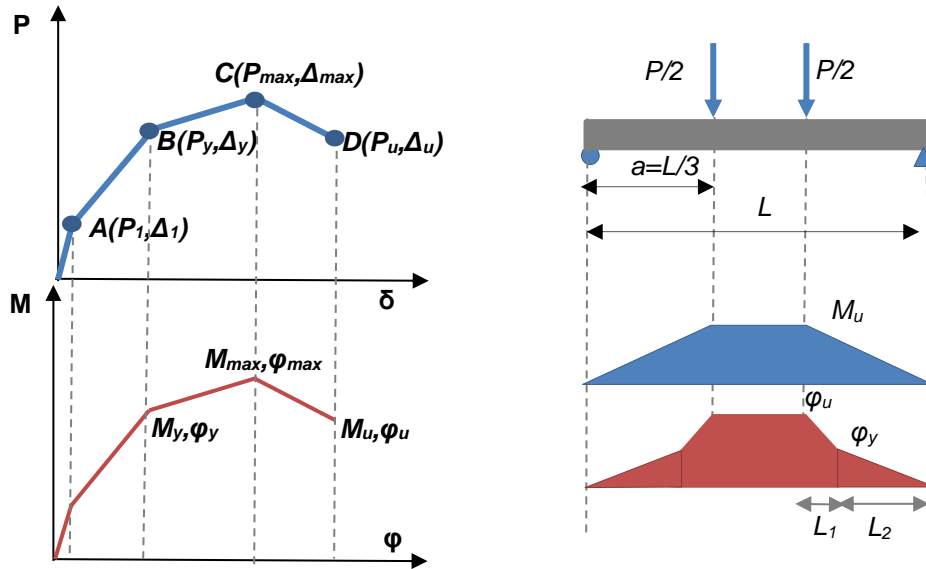

Figure 3: (a) Selection of milestone points on the load-displacement envelope. (b) To obtain the curvature – displacement relationship an assumption needs to be made regarding the "plastic hinge" zone (i.e. the zone L_1 in the figure, transitioning from the linear to the non-linear range).
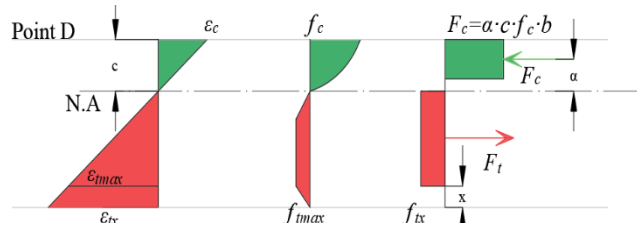
Figure 3(c): Onset of non-recoverable strength loss: When x – depth of crack penetration prevents equilibrium to be attained for moment M_u.

Other uncertainties associated with the milestone point selection are intrinsic to all simplified procedures. Some Standards and Codes prescribe this in an unambiguous manner: For example, the Canadian Standard Association[5] (CSA) adopted the inverse analysis proposed by Lopez[4] (Lopez, 2017) which refers to a five-point simplified inverse analysis for unnotched third point bending tests. The characteristic points of the load-deflection curve include the end of linearity (P_o, δ_o) that determines the initial slope of the resistance curve; Points 1 and 2 represent 75% and 40% of the initial slope, respectively. Point 3 corresponds to 97% of the peak load and Point 4 is 80% of point 3. Using the aforementioned points, cracking strength ultimate tensile strength and their corresponding strains are determined in order to establish a linearized tensile stress-strain. Basic assumptions of the method are linear elastic behaviour in compression, bilinear stress-strain tensile law until the peak and bilinear stress-crack opening behaviour at softening. The method takes into consideration the location of the crack and covers also the post-cracking behaviour. However, the method has three main restrictions: (i) is only valid for the case of third point loading, (ii) Point 3 has to be greater than Point 2 and (iii) applies only for beams with L/h=3 and L/h=4.5.

The restriction (ii) limits applicability of the approach to concretes with limited resilience range – for example it has been shown that the method is not directly applicable to prisms comprising Engineered Cementitious Composites[10](Pantazopoulou et al. 2019).

FINITE ELEMENT ANALYSIS OF GEOMETRICAL NONLINEARITIES OF 4PBT

For the most part, Finite Element analysis of UHPFRC tests are used to validate the experimental results through investigation of the nonlinear behaviour of the material. In this research, a finite element analysis was performed to study the effect of geometrical nonlinearities induced by the experimental setup, in an attempt to interpret the scatter shown in Fig. 1. To illustrate this influence on the results, constant prism dimensions are considered (75mm x 75mm x 280mm) and linear elastic material having a modulus of Elasticity of 48 GPa and Poisson's ratio of 0.18 (these correspond to measured UHPFRC properties of the materials used in obtaining Fig. 1). Tested under third point loading the typical specimen had a shear span of 75 mm, i.e., the shear span aspect ratio was =1. In the model studied, it was particularly interesting to identify the interactions between the specimen and its supports, so as to explain the observed differences in response between the tests, but also to proof test the emphasis placed by Standards recently (e.g. CSA A23.1 2019) on the details of the test setup. Thus, the entire testing mechanism including specimen, support and loading hardware were simulated in the ANSYS workbench, wherein the actual solids that represent roller and pin cylindrical supports and load impactors at third points were explicitly modelled as stainless steel shafts rather than being specified as pointwise constraints. Similarly, the steel plates under the shafts and the frictional action generated at the points of contact was a parameter of study. Steel hardware used for the testing was assigned a modulus of Elasticity equal to 193 GPa and a Poisson's ratio of 0.31. For simplicity, symmetry about the xy plane was considered so that half of the beam was analyzed. In Fig. 1 it was seen that three different commercially provided UHPFRC mixes were tested in identical triplicates, in three partner laboratories; important differences were observed between results from the three different testing teams, for otherwise identical specimens. To interpret the systematic differences between the results of the partners, every possible source of difference was explored in the present section in order to gauge its effect on the output (Figure 5). Apart from the size of the support and impactor cylinders which were different among the three partners, the type of supports (rollers on both ends with and without free longitudinal translation on either one or both ends), the type of contact (with or without friction) between all the components of the test is investigated. The available types of contact for static structural analysis and their differences are listed in Table 1. In the present study, only nonlinear types of contact were investigated.

Table 1: Types of Contacts available in ANSYS Static-Structural (ANSYS)[11]

Contact	Explanation	Type	Friction Coefficient μ	Allowed Sliding	Allowed Separation
Bonded	no sliding or separation between faces or edges is allowed	Linear	∞	no	no
No Separation	no sliding or separation between 3D faces of solids or 2D edges of plates		0	small	no
Frictional	two contacting geometries can carry shear stresses up to a certain magnitude across their interface before they start sliding relative to each other	Non-Linear	>=0	yes* (If $F_{sliding}>F_{friction}$)	yes
Frictionless	standard unilateral contact; that is, normal pressure equals zero if separation occurs		0	yes	yes
Rough	infinite friction coefficient between the contacting bodies where there is no sliding, but zero pressure if there is separation		∞	no	yes

y
x
z

Case (1)
Loading Rollers: 2.5in
Support Rollers: 1.5in

Case (2)
Loading Rollers: 1in
Support Rollers: 1in

Case (3)
Loading Rollers: 1in
Support Rollers: 2in
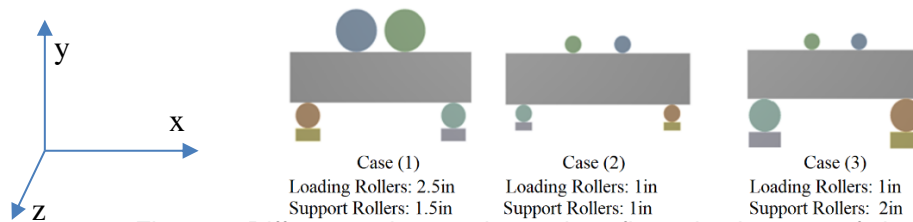
Figure 5: Differences in experimental configuration in terms of size of the rollers

Figure 5 depicts models of the three experiments compared, where the difference is in the size of the cylinder shafts used for support and impactor. The investigation focuses on: 1) size of rollers, 2) end support conditions, and 3) types of contact between specimen and the hardware, as well as between metallic components in contact with steel plates.

For the effect of the shaft diameter on the results, symmetry of supports was assumed in order to suppress other simultaneous effects owing to other variables. The analysis type was static structural with assumption of large deflections. The performance of the alternative models of the specimen were compared for midspan deflection equal to 0.05mm, which corresponded in the real experiments to nearly the attainment of peak load. In the tests, the corresponding vertical displacement at the point loads was in the range of 0.045mm. Where a frictional type of contact was used between components, the effect of friction coefficient μ was also studied for values 0.5 and 1. Frictionless contact was also considered. To study the effect of end support conditions, nonsymmetric supports were also studied modeling the entire length of the beam; in this case several combinations are considered, as depicted in Table 2 where the relevant abbreviations used henceforth to identify each analysis type is explained. Note that Cylinder 1 and 2 refer to the supporting steel shafts at the specimen ends depicted in Fig. 5.

Table2 : Cases of contact and support condition studied

Case	Support Cylinder 1	Support Cylinder 2	Contact between all bodies
RR-F	Roller	Roller	Frictional
PR-F	Roller	Pin	Frictional
PR-R	Roller	Pin	Rough

Effect of Roller Diameter

To study the effect of size of rollers, the case of roller-roller end support condition with frictional contact (μ=0.5) was used for each of the configurations in Figure 5. Taking advantage of symmetry one quarter of the beam was simulated by setting symmetry in yx and yz plane. The normal stress profile at the cross section at the midspan and under the point load is plotted in Fig. 6(a) and (b). It is observed that the effect of shaft radius is particularly important near the point of load application, where the intensity of local compressive stress increases with the decrease of radius indicating a significant stress concentration; note that case (3) had the largest size supports, and in the experiment it attained the lowest loads. The effect is attributed to the kinematic constraint imposed on the beam to wrap around the cylindrical surface of the

end shafts at the points of contact (see Fig.7). The intensity of the stress concentration is enough to locally crush the HPFRC concrete under the shafts with local compression stress levels in the order of 100 MPa (Fig. 6(b) while the midspan tensile stress is correctly quantified to be around 10 MPa (Fig. 6(a)), which was the value occurring in the tests at the peak point, just prior to cracking and subsequent strength loss. Furthermore, on account of the frictional coefficient a minor normal stress is observed at midspan, in the order of 0.2-0.3 MPa.
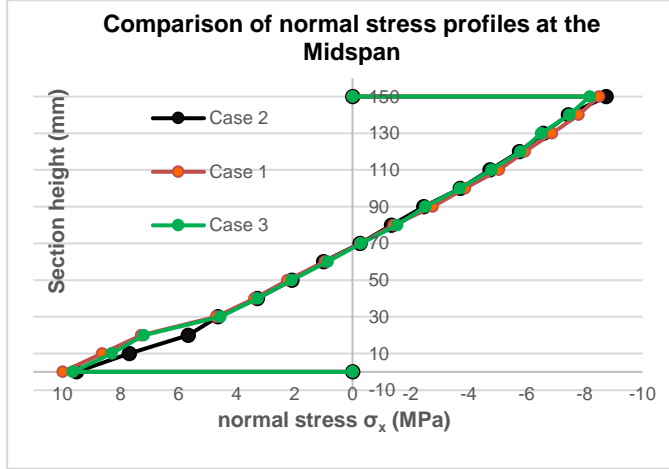
Figure 6(a): Comparison of normal stress profiles at the midspan for Cases 1, 2 and 3.
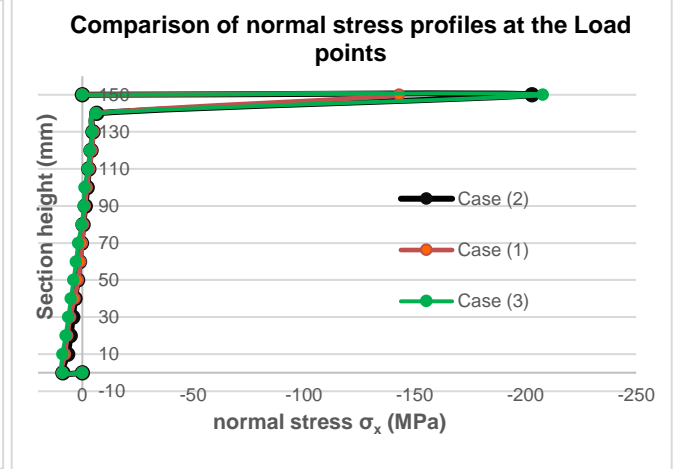
Figure 6(b): Comparison of normal stress profiles under the load for Cases 1, 2 and 3.
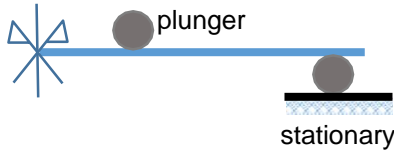
Figure 7: Local disturbance of the beams' elastica due to interference of the stationary rollers.

Table 3 lists the maximum stress values obtained for the same displacement milestone: as seen in the experiment, the three setups are organized in terms of stiffness according with the size of the support shafts. Stress fields for normal and shear stress are plotted in Fig. 8 where friction coefficient of 0.5 was considered. For Case 2 the minimum normal stress (-214MPa) was spotted on a point near the roller support while for the other two cases the minimum normal stress was spotted under the point load (-143MPa and -207MPa) . The figures depict a fundamental flaw of the prism experiments used routinely to assess tensile strength through flexural tests, by the strong evidence of the formation of a diagonal strut from impactor to support, indicating that owing to the low aspect ratio this zone performs as a D-region.

Case	Normal Stress @ L/2 $\sigma_{xx,mid}$(MPa)	Ave. Normal Stress @ h/2 $\sigma_{xx,h/2}$(MPa)	Eff. stiffness @ 0.05 mm K_{eff} (N/mm)	Max. Shear Stress τ_{xy} (MPa)	Reaction @ Roller R_y(N)	Max. frictional Stress σ_{fr}(MPa)
1: R-R	9.93	-0.2532	198.6	51.783	4414.6	24.532
2:R-R	9.52	-0.2416	190.4	62.5	4226.6	34.39
3: R-R	9.65	-0.2454	193	58.148	4265.2	32.422

Table 3: Resultant Stresses and Forces for Cases 1, 2, 3 for roller-pin end support condition

Effect of roller diameter on roller-pin support end conditions

In this section the effect of non-symmetric support conditions of the prism response is considered. Considering the contact frictional value μ=0.5, results are obtained assuming a roller in the left and pin at the right-hand side support; shaft dimensions corresponding to cases (1), (2) and (3) are used, and results

here are compared for the achieved stress intensities and distributions with their counterparts of Fig. 8 obtained considering symmetric roller supports. Table 4 summarizes the key results of the analysis. Based on the results, case (1) reaches the highest load for the displacement magnitude indicating also higher stiffness. In comparison, stress levels are higher in the roller-roller case for a given level of displacement, suggesting that given a limiting cracking strength, f_t', specimens tested under symmetric supports will crack earlier – at a lower load and displacement. This is actually consistent with the experimental observation.
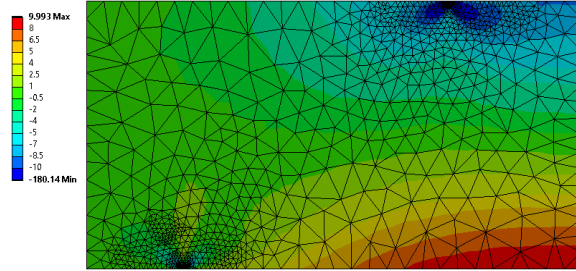
Figure 8(a): Resultant Normal Stresses for Case (1) with Roller-Roller
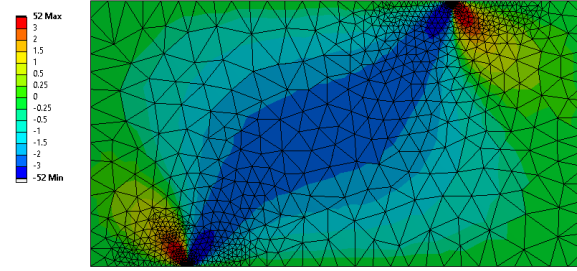
Figure 8(b): Resultant Shear Stresses for Case (1) Roller-Roller
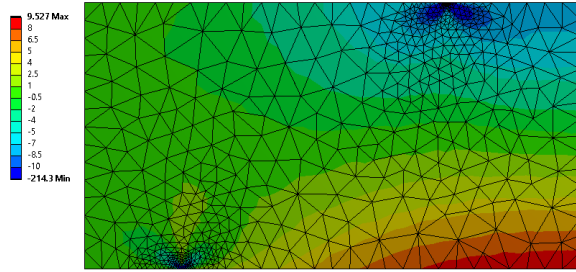
Figure 8(c): Resultant Normal Stresses for Case (2) with Roller-Roller
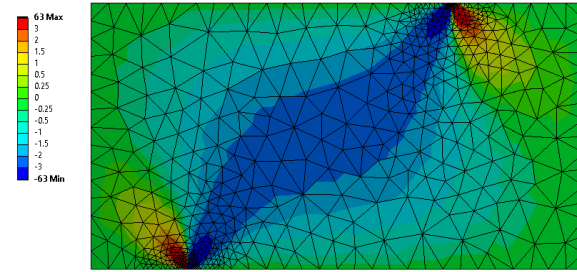
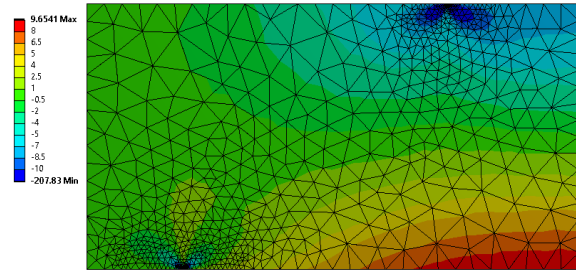Figure 8(d): Resultant Shear Stresses for Case (2) Roller-Roller

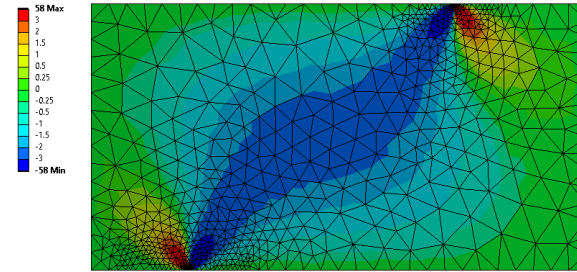Figure 8(e): Resultant Normal Stresses for Case (3) with Roller-Roller

Figure 8(f): Resultant Shear Stresses for Case (3) Roller-Roller

Table 4: Resultant Stresses (MPa) and Forces (N) for Cases 1,2,3 for roller-pin end support condition

Case	Normal Stress at L/2 $\sigma_{xx,mid}$	Av. Normal Stress at h/2 $\sigma_{xx,h/2}$	Max. Shear Stress τ_{xy}	Reaction at Roller R_y	Reaction at Pin P_y	Reaction at Pin P_x	Max. frictional Stress σ_{fr}
1:R-P	9.2089	-0.30703	43.8	4121.6	4115.88	0.316	13.549
2:R-P	8.49	-0.2	45.85	3794.17	3805.55	0.2638	23.073
3:R-P	9.94	-0.2314	45.9	3935.7	3958.9	0.2345	14.263

Frictional Influences

The effect of different types of contacts was studied only on Case (1). To show the effect of friction, frictional contact with allowed penetration of the rollers in the specimen and different friction coefficients was studied. From Table 5 it can be assumed that frictional effects are visible only in case of asymmetric support conditions as on the horizontal reaction component of the pin is increased with the increase of the frictional coefficient.

Figure 9(a): Normal Stresses, Case (1), Roller-Pin
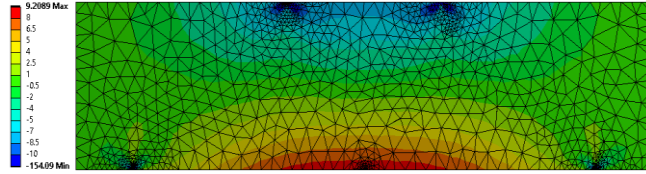
Figure 9(b): Shear Stresses, Case (1), Roller-Pin
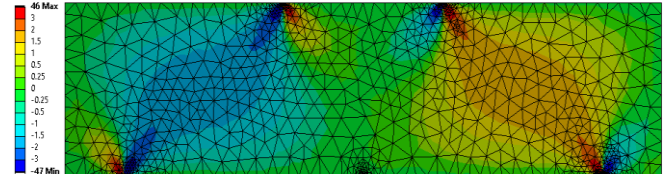
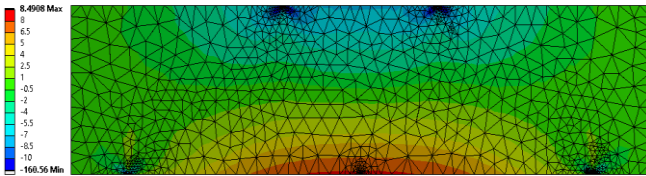Figure 9(c): Normal Stresses, Case (2), Roller-Pin

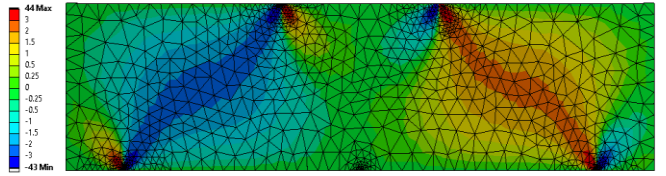Figure 9(d): Shear Stresses, Case (2), Roller-
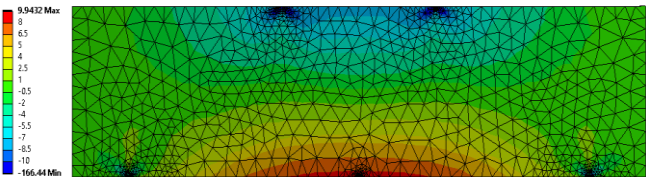

Figure 9(e): Normal Stresses, Case (3), Roller-Pin
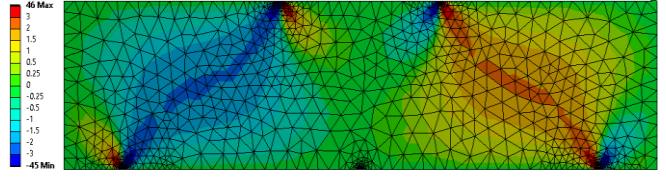

Figure 9(f): Shear Stresses, Case (3), Roller-Pin

Table 5: Resultant stresses for nonlinear types of contact for Case 1

Friction Coefficient μ	Case	Normal Stress @L/2 $\sigma_{xx,mid}$	Normal Stress @h/2 $\sigma_{xx,h/2}$	Max Shear Stress $\tau_{xy,max}$	Reaction @ Roller R_y	Reaction @ Pin P_y	Reaction @ Pin P_x	Max Frictional stress σ_{fr}
∞	PR-R	9.93	-0.3196	61.924	4567.66	4568.586	2.824	61.924
1	PR-F	10.022	-0.308	50.103	4495.37	4479.667	0.5162	41.494
0.5	PR-F	10.1	-0.3069	48.892	4471.716	4466.665	0.4236	29.764

The Direct Tension Specimen

For comparison purposes one eighth of the beam was simulated in direct tension (37.5mm x37.5mm x140mm). As in the case of four-point bending tests, a wedge of dimensions 37.5mm x17.5mm x42.5mm was also simulated and a frictional contact of 0.5 and 1 was assumed to avoid premature sliding at the interface. A displacement of 0.1mm was applied on the wedge. The configuration and results in terms of stresses and strain distribution are shown in Fig. 10. The resultant stress at the midsection for μ=0.5 was 4.7MPa while the strain was 9.8617×10^{-5} mm/mm. For μ=1 the stress was 9.45MPa and the strain 1.9699×10^{-4} mm/mm. Figure 10 also illustrates the problematic nature of the test in terms of the intense stress concentrations under the area that is in contact with the steel wedge and nonuniform strain distribution along specimen's length.
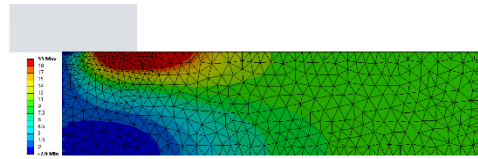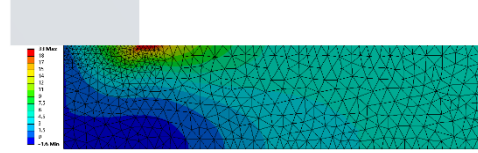
Figure 10 (a): Normal stress for μ=1.

Figure 10 (b): Normal stress for μ=0.5

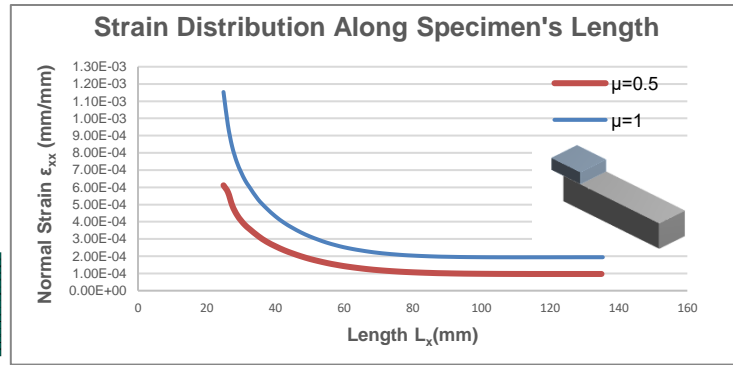

Figure 10 (c): Normal stress for μ=0.5

CONCLUSIONS

The objective of the research was to evaluate the relevance between results from UHPFRC direct tension test and flexural tests conducted as per the established relevant testing procedures. The geometrical nonlinearities induced by the experimental configuration of four-point bending test were studied through detailed finite element simulations. Parameters such as friction, roller diameter and end support conditions were investigated. Based on the results it was concluded that: (i) decrease of rollers' radius creates high stress concentration and distortion of the normal stress profile under the point of application of the load, (ii) steep diagonal strut action is developed for cases of impactor/roller diameter ratio higher than 1, (iii) Frictional influences are more visible in the asymmetric case of pin-roller and (iv) Pin-Roller end support condition creates a slightly unsymmetric model with the horizontal force reaction to depend on the generated frictional stresses. The effect is more intense in case of smaller rollers (Case 2) and (iv) The correlation between results obtained from direct tension and bending experiments is not straightforward, because the strain distribution in the direct tension case is highly nonlinear and depends also on the frictional action exerted by the grips.

REFERENCES

1. ACI 544R-17. *Report on Measuring Mechanical Properties of Hardened Fiber-Reinforced Concrete* ACI Committee 544
2. AFNOR NF EN 13670/CN (2013). Exécution des Structures en Béton – Complément National à la Norme NF EN 13670
3. Yang, Y. (2019). A Thesis Report: Tensile Behavior of Ultra- High-Performance Steel Fiber Reinforced Concrete.
4. Lopez, J. (2017). A Thesis Report: Characterization of The Tensile Behaviour of UHPFRC by Means of Four-Point Bending Tests.
5. Canadian Standards Association (2019). Annex U A23.1: Ultra-high-performance concrete (UHPC).
6. Baby, F., Graybeal, B., Marchand, P., & Toutlemonde, F. (2012). Proposed Flexural Test Method Associated Inverse Analysis for Ultra High-Performance Fiber Reinforced Concrete. *ACI Materials Journal*, 109(5), 545-556
7. Rigaud, S., Chanvillar, G., and Chen, J. (2011). Characterization of Bending and Tensile Behavior of Ultra-High-Performance Concrete Containing Glass Fibers. *6th International Symposium on High Performance Fiber Reinforce Cement Composites,* 373-380.
8. Qian, S., and Li, V. (2007). Simplified Inverse Method for Determining the Tensile Strain Capacity of Strain Hardening Cementitious Composites. *Journal of Advanced Concrete Technology*, 5(2), 235-246
9. Georgiou, A. V. and Pantazopoulou S. J. (2016). Effect of fiber length and surface characteristics on the mechanical properties of cementitious composites. *Construction and Building Materials,* 125, 1216-1228
10. Pantazopoulou, S. J., Palermo, D., Yang, Y., Eshghi, N., Saikali, R. and Chasioti, S. (2019) Technical Report: Development of Specifications for Determining the Tensile Behaviour of UHPFRC Materials for Structural Applications in Highway Bridges,
11. ANSYS *® Academic Research Mechanical, Release 19.2, Help System, Static Structural Analysis Guide, ANSYS, Inc.*